# Supplementary Material: Detailed Formulation of the Robust Optimal Control Problem

Tomás Ochoa, Balarko Chaudhuri, and Mark O'Malley

## I. Preface

This supplementary document provides the complete mathematical formulation of the robust optimal control problem (ROCP) presented in the main manuscript [1]. The aim of the ROCP formulation is to establish a mathematical optimization program that seeks to enhance the robust large-signal dynamic performance of inverter-dominated power systems (IDPSs) through the coordinated selection of control architectures and the corresponding parameter tuning of inverter-based resources (IBRs). The purpose of this document is to present, in explicit and self-contained form, the modeling components that define this optimization problem.

The aim of this document is to provide a precise and transparent mathematical reference for the ROCP formulation. The ROCP transcription, min–max decomposition, and solution procedure are intentionally excluded, as they are fully described in the main manuscript and documented in the accompanying implementation available at **github.com/Aerlio/ROC-of-IDPS**.

The formulation is developed progressively by detailing the models used to represent IBRs, dispatch mechanisms, and large-signal disturbances in Sections III, IV, and V, respectively. Each component is presented explicitly at the equation level and assembled into a unified dynamic model of the IDPS in Section VI, expressed as a system of differential–algebraic equations (DAEs). The dynamic error metric,

T. Ochoa, B. Chaudhuri, and M. O'Malley are with the Department of Electrical and Electronic Engineering, Imperial College London, London, SW7 2AZ, UK (e-mail: t.ochoa@imperial.ac.uk).

which constitutes the objective function of the ROCP, is then introduced in Section VII. Finally, the ROCP, as stated in [1], is restated in full to render this document mathematically self-contained.

For completeness and mathematical clarity, the nomenclature adopted here may differ from that of the main manuscript. Additional symbols and refined definitions are introduced where necessary to provide a fully explicit and internally consistent formulation.

## II. Preliminaries

### A. Notation

For clarity, we omit explicit time dependence in the notation when convenient; however, it remains implicit and can be inferred from the context. Bold italic symbols, $\boldsymbol{X}$, denote vectors and matrices, while calligraphic symbols, $\mathcal{X}$, represent vectors and matrices composed of constant parameter values. Furthermore, Fraktur symbols, $\mathfrak{X}$, denote admissible sets. In particular, the symbols $h$ and $K$ are used to represent control state variables and control parameters, respectively. Transpose is denoted by $\boldsymbol{x}^T$, magnitude by $|\cdot|$, and the imaginary unit by $\jmath$. Element-wise operations on vectors and matrices are denoted using Hadamard operators: multiplication with $\odot$, division with $\oslash$, squaring with $\boldsymbol{x}^{\circ 2}$, and inversion with $\boldsymbol{x}^{\circ -1}$. Particularly, $\frac{d}{dt}\boldsymbol{x}$ denotes element-wise time differentiation.

### B. Assumptions

We list the assumptions made in this work:

- The system operates under balanced three-phase conditions.
- Transformers are modeled as resistive-inductive branches, while transmission lines are represented using lumped $\pi$-section equivalents.
- Loads are modeled as constant-impedance [2].
- Fast inverter switching dynamics are represented using a dynamic average-value modeling approach [3], [4].
- Following [5], the IBRs' DC sides are modeled with a DC-link capacitor and a controllable current source regulated by a delayed proportional-integral (PI) controller to maintain nominal DC voltage.

### C. Per-Unit Values for Power System

To implement a per-unit system, pu, following the approach used in References [3], [6], we define base quantities, denoted with the subscript $b$, for both the AC power system and the IBRs DC-sides as shown in Table I. We arbitrarily define the base values for three-phase rating, $S_b$ in VA, frequency, $f_b$

in Hz, and nominal line-to-neutral voltage amplitude for each bus, $V_b = \hat{V}_s$ in V. Note that while angular velocities, $\omega$, are expressed in pu, angle and time variables are expressed in rad and sec, respectively.

TABLE I
BASE QUANTITIES CALCULATION

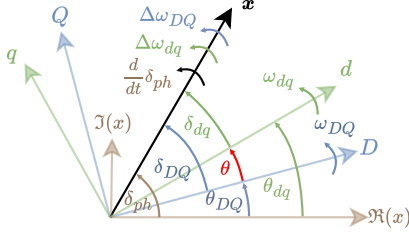| Quantity | AC Power System | IBRs DC-side |
|---|---|---|
| Power | $S_b = \frac{3}{2} V_b I_b$ | |
| Frequency | $\omega_b = 2\pi f_b$ | |
| Voltage | $V_b = \hat{V}_s$ | $V_{b-dc} = 2V_b$ |
| Current | $I_b = \frac{2}{3}\frac{S_b}{V_b}$ | $I_{b-dc} = \frac{3}{4} I_b$ |
| Impedance | $Z_b = \frac{V_b}{I_b}$ | $Z_{b-dc} = \frac{8}{3} Z_b$ |
| Capacitance | $C_b = \frac{1}{Z_b \omega_b}$ | $C_{b-dc} = \frac{3}{8} C_b$ |
| Inductance | $L_b = \frac{Z_b}{\omega_b}$ | $L_{b-dc} = \frac{8}{3} L_b$ |

### D. Reference Frames



Fig. 1. Global and local reference frames.

*1) Three-phase abc signals and space phasors:* Our analysis is centred on balanced systems, characterized by the condition that the sum of the three-phase time-domain signals, $\boldsymbol{x}_{abc} = [x_a, x_b, x_c]^T$, equals zero, i.e., $x_a + x_b + x_c = 0$. This balance assumption allows to represent these three-phase signals by two independent signals without loss of generality. One commonly used representation (termed as space phasor in [7]) defines a time-domain complex-valued scalar as:

$$\boldsymbol{x}_{ph} = \begin{bmatrix} 1 & e^{j\frac{2\pi}{3}} & e^{j\frac{4\pi}{3}} \end{bmatrix} \boldsymbol{x}_{abc} \triangleq |\boldsymbol{x}_{ph}|\angle\delta_{ph}, \quad (1)$$

where $|\boldsymbol{x}_{ph}|$ and $\delta_{ph}$ are the time-varying space phasor magnitude and angle w.r.t. the complex plane, respectively, as shown in Fig. 1. Note that the space phasor angle time-derivative, $\frac{d}{dt}\delta$, is equal to the three-phase sinusoidal signals angular velocity in rad/sec.

*2) Global DQ-frame:* Due to the sinusoidal nature of AC power system quantities and for the ease of analysis, space phasors are commonly projected onto a common reference frame rotating at a fixed angular velocity, $\omega_{DQ}$, set at 1 (pu). Thus, as $\frac{d}{dt}\theta_{DQ} = \omega_b \omega_{DQ}$, the $DQ$-frame time-domain angle w.r.t. the complex plane as shown in Fig. 1 is:

$$\theta_{DQ} = \theta_0 + \omega_b \omega_{DQ} t, \quad (2)$$

where $\theta_0$ is the starting time value.

To project the three-phase signals into the global $DQ$-frame, we employ the popularly known standard (amplitude-invariant) Park transformation, defined as [8]:

$$\Gamma(\theta_{DQ}) = \frac{2}{3} \begin{bmatrix} cos(\theta_{DQ}) & -sin(\theta_{DQ}) \\ cos(\theta_{DQ} - \frac{2\pi}{3}) & -sin(\theta_{DQ} - \frac{2\pi}{3}) \\ cos(\theta_{DQ} + \frac{2\pi}{3}) & -sin(\theta_{DQ} + \frac{2\pi}{3}) \end{bmatrix}^T. \quad (3)$$

An useful property of the standard Park transformation is that for an arbitrary balanced signal in the abc-frame, $\boldsymbol{x}_{abc}$, it holds that [9]:

$$\frac{d}{dt}\boldsymbol{x}_{abc} = \Gamma^{-1}(\theta_{DQ})\left(\frac{d}{dt}\boldsymbol{x}_{DQ} - \mathcal{J}\omega_b \boldsymbol{x}_{DQ}\right), \quad (4)$$

where $\boldsymbol{x}_{DQ} = [x_D, x_Q]^T$ is a DQ signal and $\mathcal{J} = \begin{bmatrix} 0 & 1 \\ -1 & 0 \end{bmatrix}$ is the 90° rotation matrix.

For a given variable in the $DQ$-frame, $\boldsymbol{x}_{DQ}$, its angle w.r.t. the $DQ$-frame can be obtained from $\delta_{DQ} = tan^{-1}(x_Q, x_D)$, where $tan(\cdot)$ is the tangent function. Thus, if the angular velocity of $\boldsymbol{x}_{DQ}$ w.r.t. the $DQ$-frame is $\Delta\omega_{DQ}$, it implies that the three-phase sinusoidal signals angular velocity is $\omega_{DQ} + \Delta\omega_{DQ}$, where:

$$\frac{d}{dt}\delta_{DQ} = \frac{x_D \frac{d}{dt}x_Q - x_Q \frac{d}{dt}x_D}{x_D^2 + x_Q^2} = \omega_b \Delta\omega_{DQ}, \quad (5)$$

being easily demonstrable that if the time differentiations of $x_D$ and $x_Q$ are zero, the associated three-phase sinusoidal signals are oscillating at $\omega_{DQ}\omega_b$ in rad/sec.

*3) Local dq-frames:* Local $dq$-frames are device-specific rotating reference frames. In contrast to the global $DQ$-frame, the angular velocity of a local $dq$-frame, $\omega_{dq}$, can change over time. Typically, each inverter operates in a local $dq$-frame, which angular velocity is determined by the inverter's Phase Locked Loop (PLL) for GFL control structures or by the Power Synchronization Loop (PSL) for GFM control structures. The angle difference between the local $dq$-frame w.r.t. the global $DQ$-frame, $\theta$, is defined by:

$$\theta = \theta_{dq} - \theta_{DQ} = \delta_{DQ} - \delta_{dq}, \quad (6)$$

as represented in Fig. 1.

To provide a consistent system-wide transformation between the $dq$- and $DQ$-frames, define the rotation matrix:

$$R(\theta) = \begin{bmatrix} cos(\theta) & -sin(\theta) \\ sin(\theta) & cos(\theta) \end{bmatrix}. \quad (7)$$

It follows that $\boldsymbol{x}_{DQ} = R(\theta)\boldsymbol{x}_{dq}$ and $R^{-1}(\theta) = R(-\theta)$, where $\boldsymbol{x}_{dq} = [x_d, x_q]^T$. By replacing $\delta_{DQ}$ and $\boldsymbol{x}_{DQ}$ with $\delta_{dq}$ and $\boldsymbol{x}_{dq}$ in (5), respectively, we can obtain $\Delta\omega_{dq}$.

Note that to further expand our work to consider unbalanced operation, it is necessary to include the zero-sequence component to the $DQ$- and $dq$-frames [8].

### III. INVERTER BASED RESOURCE MODEL

In this section, we outline the model of an individual IBR. As shown in Fig. 2, the model is divided into physical and control layers. The physical layer includes the DC and AC sides connected through a switching stage, a representation of

the DC energy source's response time, and a power measurement filter. The control layer comprises both DC- and AC-side controllers, with the latter configurable to implement various AC-side control structures, as detailed in Section III-B2.
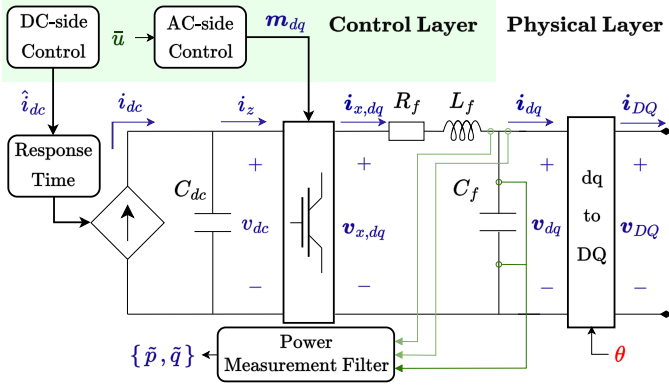


Fig. 2. Inverter model including physical and control layers.

## A. Physical Layer

*1) Electric Circuit:* Consider the electric circuit dynamics as:

$$\boldsymbol{v}_{x,dq} = v_{dc}\boldsymbol{m}_{dq}, \tag{8a}$$

$$i_z = m_d i_{x,d} + m_q i_{x,q}, \tag{8b}$$

$$\frac{1}{\omega_b}\frac{d}{dt}v_{dc} = C_{dc}^{-1}\left(i_{dc} - i_z\right), \tag{8c}$$

$$\frac{1}{\omega_b}\frac{d}{dt}\boldsymbol{v}_{dq} = C_f^{-1}\left(\boldsymbol{i}_{x,dq} - \boldsymbol{i}_{dq}\right) + \omega_{dq}\mathcal{J}\boldsymbol{v}_{dq}, \tag{8d}$$

$$\frac{1}{\omega_b}\frac{d}{dt}\boldsymbol{i}_{x,dq} = L_f^{-1}\left(\boldsymbol{v}_{x,dq} - \boldsymbol{v}_{dq} - R_f \boldsymbol{i}_{x,dq}\right) + \dots$$
$$\dots \omega_{dq}\mathcal{J}\boldsymbol{i}_{x,dq}, \tag{8e}$$

where $C_{dc}$ is the DC-link capacitance. $R_f$, $L_f$, and $C_f$ are the filter resistance, inductance, and capacitance values, respectively. Moreover, $v_{dc}$ denotes the DC-link voltage, $i_{dc}$ is the DC source current injection, $i_z$ is the DC-side current at the switching stage, $\boldsymbol{v}_{x,dq} = [v_{x,d}, v_{x,q}]^T$ and $\boldsymbol{i}_{x,dq} = [i_d, i_q]^T$ are the AC-side voltage and current at the switching stage, $\boldsymbol{m}_{dq} = [m_d, m_q]^T$ denotes the modulation signal, and $\boldsymbol{v}_{dq} = [v_d, v_q]^T$ and $\boldsymbol{i}_{dq} = [i_d, i_q]^T$ are the AC-side node voltage and node current. Meanwhile, $\omega_{dq}$ is the local $dq$-frame angular velocity generated by a PSL or PLL dependent on the AC-side control structure.

*2) Response Time:* Consider the dynamics related to the DC energy source response time as:

$$\frac{d}{dt}i_{dc} = \mathcal{T}_{dc}^{-1}(\hat{i}_{dc} - i_{dc}), \tag{9}$$

where $\mathcal{T}_{dc}$ is the response time associated with the IBR's power source. Moreover, $\hat{i}_{dc}$ is the DC current reference signal.

*3) Power Measurement Filter:* The instantaneous DC-side active power and AC-side active and reactive power at the IBR's node are calculated as:

$$p_{dc} = v_{dc}i_z \,, \ \ p = v_d i_d + v_q i_q \,, \ \ q = v_q i_d - v_d i_q. \tag{10}$$

To remove the high frequency components, the computed AC active and reactive power values are filtered through a Low-Pass Filter (LPF) as follows [9]:

$$\frac{d}{dt}\tilde{p} = K_c(p - \tilde{p})\,, \ \ \frac{d}{dt}\tilde{q} = K_c(q - \tilde{q}), \tag{11}$$

where $K_c$ is the cut-off frequency parameter. Moreover, $\tilde{p}$ and $\tilde{q}$ are the LPF outputs for the active and reactive power measurements, respectively.

## B. Control Layer

*1) DC-side Control:* The DC-side control consists on a Proportional-Integral (PI) controller which regulates the DC voltage to its nominal value, $v_{dc,0}$, and a power injection and feed-forward loss compensation term [5]. Consider the DC voltage controller dynamics as:

$$\frac{d}{dt}h_{dc} = K_{dc,I}\left(v_{dc,0} - v_{dc}\right), \tag{12a}$$

$$\hat{i}_{dc} = K_{dc,P}\left(v_{dc,0} - v_{dc}\right) + h_{dc} + \frac{p_{\text{ref}} + p_{dc} - p}{v_{dc,0}}, \tag{12b}$$

where $K_{dc,P}$ and $K_{dc,I}$ are the PI parameter gains and $h_{dc}$ is the DC-side controller integrator state. Moreover, $p_{\text{ref}}$ is the active power reference signal. Thus, the first and second term in (12b) corresponds to the PI terms. Meanwhile, the third term corresponds to the power injection and feed-forward loss compensation, where the difference between the DC and AC active powers compensates the filter losses.

*2) AC-Side Control Structure:* The literature offers a variety of control structures for AC-side control. Figure 3 illustrates a flexible architecture capable of accommodating multiple popular control structures. As shown, this flexible architecture can be configured using a set of integer indicators, $u = \{u_{\text{GFL}}, u_{\text{GFM}}, u_\theta\}$, to select among well-known control structures usually categorized as GFL or GFM [5], [10], [11].

In this work, we limit our focus to two configurations: (i) GFL with droop loop model and (ii) GFM with droop model. For a broader overview of AC-side control structures, we refer the reader to [10].

*3) GFM Model:* A GFM model is only included if $u_\theta = 1$. These do not require a PLL and its output serve as an input for a voltage controller. The GFM model selection is based on the value of $u_{\text{GFM}}$. Specifically, the GFM droop model is described as:

$$\frac{d}{dt}\theta_{dq} = \omega_b \omega_{dq}, \tag{13a}$$

$$\omega_{dq} = K_{p/\omega}(p_{\text{ref}} - \tilde{p}) + \omega_0, \tag{13b}$$

$$\hat{v}_d = K_{q/v}(\tilde{q} - q_{\text{ref}}) + v_0\,, \quad \hat{v}_q = 0, \tag{13c}$$

where $K_{p/\omega}$ and $K_{q/v}$ are the droop parameters and $p_{\text{ref}}$ and $q_{\text{ref}}$ are the active and reactive power reference signals. Moreover, $\theta_{dq}$ and $\omega_{dq}$ are the local $dq$-frame angle in `rad` and velocity in `pu`, respectively, $\omega_0 = 1\,(\text{pu})$ and $v_0 = 1\,(\text{pu})$ are the nominal angular velocity and nominal voltage magnitude. The droop model generates a voltage magnitude output which is aligned with the $d$-axis, $\hat{v}_d$, thus, $\hat{v}_q = 0$.
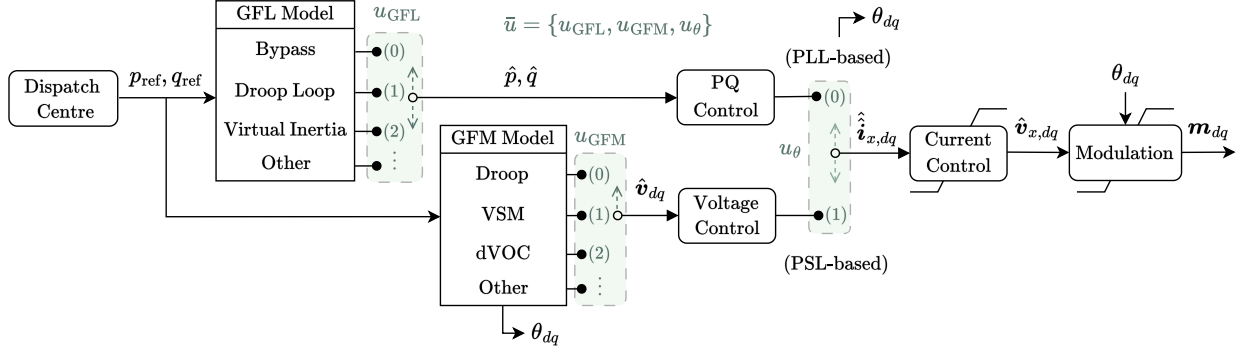
Fig. 3. Configurable AC-side control architecture of an IBR.

*4) GFL Models:* A GFL model is included only if $u_\theta = 0$, these require a PLL and its outputs, $\hat{p}$ and $\hat{q}$, will serve as an input for a PQ controller. The GFL model selection is based on the value of $u_{\text{GFL}}$. Specifically, the GFL droop loop model is described as:

$$\hat{p} = K_{\omega/p}(\omega_0 - \omega_{dq}) + p_{\text{ref}}, \tag{14a}$$

$$\hat{q} = K_{v/q}(v_0 - |\boldsymbol{v}_{dq}|) + q_{\text{ref}}, \tag{14b}$$

where $K_{\omega/p}$ and $K_{v/q}$ are the droop loop parameters.

*5) PLL Model:* A PLL model is only included if $u_\theta = 0$. The PLL outputs $\omega_{dq}$ and $\theta_{dq}$ are the local $dq$-frame angle and velocity, respectively. Consider the PLL dynamics as:

$$\frac{d}{dt}h_{pll} = -K_{pll,I}v_q, \tag{15a}$$

$$\omega_{dq} = -K_{pll,P}v_q + h_{pll} + \omega_0 , \quad \frac{d}{dt}\theta_{dq} = \omega_b\omega_{dq}, \tag{15b}$$

where $K_{pll,P}$ and $K_{pll,I}$ are the PLL PI parameters. Moreover, $h_{pll}$ is PLL integrator state.

*6) Current Control and Modulation:* Independent of the control structure configuration, IBRs are considered to have a cascaded current controller and modulation block. To incorporate current saturation, we note that a wide variety of direct and indirect current saturation methods exist in the literature [12]. Without loss of generality, we consider only the circular current-reference saturation method, formulated as:

$$\hat{\boldsymbol{i}}_{x,dq} = \alpha\hat{\hat{\boldsymbol{i}}}_{x,dq} , \quad \alpha = f_{\text{UB}}(\frac{i_{\text{x,max}}}{|\hat{\hat{\boldsymbol{i}}}_{x,dq}|}, 1), \tag{16a}$$

$$f_{\text{UB}}(x, x_{\text{max}}) = \frac{1 + x - \sqrt{(x - x_{\text{max}})^2}}{2}, \tag{16b}$$

where $i_{\text{x,max}}$ is the IBRs maximum current, usually around 1.1-1.4 times the nominal current if not oversized. Moreover, $\hat{\hat{\boldsymbol{i}}}_{x,dq} = [\hat{\hat{i}}_{x,d}, \hat{\hat{i}}_{x,q}]^T$ is the reference current signal which comes from either a PQ or voltage controller and $\hat{\boldsymbol{i}}_{x,dq} = [\hat{i}_{x,d}, \hat{i}_{x,q}]^T$ is the saturated current reference. In (16), $f_{\text{UB}}(x, x_{\text{max}})$ is an upper-bound saturation function that limits $x$ to values less than or equal to $x_{\text{max}}$ [13]. Thus, if $|\hat{\hat{\boldsymbol{i}}}_{x,dq}| \leq i_{\text{x,max}}$, no saturation is applied and $\alpha$ is set to 1; otherwise, $\alpha$ is given by $\frac{i_{\text{x,max}}}{|\hat{\hat{\boldsymbol{i}}}_{x,dq}|}$.

The current controller and modulation dynamics are described as:

$$\frac{d}{dt}\boldsymbol{h}_i = K_{i,I}\left(\hat{\boldsymbol{i}}_{x,dq} - \boldsymbol{i}_{x,dq}\right), \tag{17a}$$

$$\hat{\boldsymbol{v}}_{x,dq} = K_{i,P}\left(\hat{\boldsymbol{i}}_{x,dq} - \boldsymbol{i}_{x,dq}\right) + \boldsymbol{v}_{dq}$$
$$+ \boldsymbol{h}_i + R_f\boldsymbol{i}_{x,dq} - \mathcal{J}\omega_{dq}L_f\boldsymbol{i}_{x,dq}, \tag{17b}$$

$$\hat{\boldsymbol{m}}_{dq} = \frac{\hat{\boldsymbol{v}}_{x,dq}}{v_{dc,0}}, \tag{17c}$$

where $K_{i,P}$ and $K_{i,I}$ are the PI current control parameters. Moreover, $\boldsymbol{h}_i = [h_{i,d}, h_{i,q}]^T$ is the bi-dimensional current controller integrator state for the signal tracking error of the saturated current reference.

*7) PQ and Voltage Control:* Depending on the selection of $u_\theta$, either a PQ or a voltage controller may be required. In both cases, the controller output serves as the input to the current controller. To prevent the integrator in the current controller from accumulating excessive error during over-current saturation events, an anti-windup mechanism is incorporated [14]. Specifically, the difference between the saturated and non-saturated current reference signals is added to the integrator states for both the PQ and voltage controllers. This difference is zero unless $\alpha \neq 1$.

If $u_\theta = 0$, consider the PQ controller defined by:

$$\frac{d}{dt}\boldsymbol{h}_{pq} = K_{pq,I}([\hat{p} - \tilde{p}, \tilde{q} - \hat{q}]^T + \hat{\boldsymbol{i}}_{x,dq} - \hat{\hat{\boldsymbol{i}}}_{x,dq}), \tag{18a}$$

$$\hat{\hat{\boldsymbol{i}}}_{x,dq} = K_{pq,P}[\hat{p} - \tilde{p}, \tilde{q} - \hat{q}]^T + \boldsymbol{h}_{pq}, \tag{18b}$$

where $K_{pq,P}$ and $K_{pq,I}$ are the PI PQ control parameters. Moreover, $\boldsymbol{h}_{pq} = [h_{pq,p}, h_{pq,q}]^T$ is the bi-dimensional PQ controller integrator state.

If $u_\theta = 1$, consider the AC voltage controller defined by:

$$\frac{d}{dt}\boldsymbol{h}_v = K_{v,I}(\hat{\boldsymbol{v}}_{dq} - \boldsymbol{v}_{dq} + \hat{\boldsymbol{i}}_{x,dq} - \hat{\hat{\boldsymbol{i}}}_{x,dq}), \tag{19a}$$

$$\hat{\hat{\boldsymbol{i}}}_{x,dq} = K_{v,P}(\hat{\boldsymbol{v}}_{dq} - \boldsymbol{v}_{dq}) + \boldsymbol{h}_v - \mathcal{J}\omega_{dq}C_f\boldsymbol{v}_{dq} + \boldsymbol{i}_{dq}, \tag{19b}$$

where $K_{v,P}$ and $K_{v,I}$ are the PI voltage control parameters. Moreover, $\boldsymbol{h}_v = [h_{v,d}, h_{v,q}]^T$ is the bi-dimensional voltage controller integrator state.

## C. IBR Integration into a Network Model

To transform the IBR node voltage and current, $v_{dq}$ and $i_{dq}$, into the $DQ$-frame, we use the frame transformation defined in (7), where $\theta = \theta_{dq} - \theta_{DQ}$. To integrate all IBRs into a network model as described in Section VI, the individual IBR node voltages and currents are collected into the vectors $\boldsymbol{v}_D^{\text{IBR}}$, $\boldsymbol{v}_Q^{\text{IBR}}$, $\boldsymbol{i}_D^{\text{IBR}}$, and $\boldsymbol{i}_Q^{\text{IBR}}$, each sized according to the total number of IBRs in the system. Similarly, all other individual IBR variables and algebraic expressions, $\boldsymbol{x}$, are aggregated into vectors of the form $\boldsymbol{x}^{\text{IBR}}$.

## D. Control Design Admissible Sets

Constraining the control design space to well-established architectures and parameter ranges is essential for ensuring that IBR controllers comply with system-level requirements. This approach not only ensures practical relevance but also builds on prior research and established engineering practices. Furthermore, by imposing clear bounds on control structures and parameters.

This work focuses on two control configurations: (i) Grid-Following (GFL) with a droop loop model, and (ii) Grid-Forming (GFM) with a droop model. In this document, the control configuration for each IBR is specified by setting the integer indicator variable $u_\theta$ to 0 or 1, corresponding to the configuration (i) or (ii), respectively. This work focuses on two control configurations: (i) Grid-Following (GFL) with a droop loop model, and (ii) Grid-Forming (GFM) with a droop model. As introduced in Part I, the control configuration for each IBR is specified by setting the integer indicator variable $u_\theta$ to 0 or 1, corresponding to the configuration (i) or (ii), respectively.

Accordingly, the admissible control-architecture set is specified as:

$$\mathcal{A}^{\text{u}} \coloneqq \{\boldsymbol{u} \mid \boldsymbol{u}_\theta \in \{0,1\}\}. \tag{20}$$

To ensure comparable control parameters across both configurations, we exploit the reciprocity between the two control structures and introduce a unified notation for the outer control parameters, regardless of the selected configuration:

$$K^{\text{P}} = K_{p/\omega} = \frac{1}{K_{\omega/p}} \quad , \quad K^{\text{Q}} = K_{q/v} = \frac{1}{K_{v/q}}, \tag{21}$$

where $K^{\text{P}}$ and $K^{\text{Q}}$ denote the unified outer control parameters for each IBR. Moreover, for each IBR, $K_{p/\omega}$ and $K_{q/v}$ are the GFM droop parameters and $K_{\omega/p}$ and $K_{v/q}$ represent their GFL counterparts.

Accordingly, the admissible control-parameters set is specified as:

$$\mathcal{A}^{\text{K}} \coloneqq \Big\{ \boldsymbol{K} \;\Big|\; \boldsymbol{K} \coloneqq \big\{ \boldsymbol{K}^{\text{P}}, \boldsymbol{K}^{\text{Q}} \big\}, \tag{22}$$
$$\boldsymbol{K}^{\text{P}} \in \left[10^{-3}, 10^{-1}\right], \boldsymbol{K}^{\text{Q}} \in \left[10^{-3}, 10^{-1}\right]. \Big\}$$

## IV. DISPATCH MECHANISMS

System operators send reference signals to selected generators to meet demand economically while maintaining stability and satisfying operational and reliability requirements. A key tool for this task is the Economic Dispatch (ED) program, which determines the most cost-effective generation levels by considering generation costs, system constraints, and operational limits. ED is typically run on a short-term basis, every few minutes to an hour. Another important dispatch mechanism is Automatic Generation Control (AGC), which operates every few seconds. The primary objective of AGC is to maintain system frequency within a narrow range around its nominal value. Traditional AGC implementations rely on simple regression-based models driven by local frequency measurements [15]. AGC is deemed a re-dispatch process, as it inherits reactive reference signals from the ED solution [16].

Before proceeding, let the reference signals vector, $\boldsymbol{r}^{\text{n}}$, consist of ED-based reference values, $\boldsymbol{r}^{\text{ED}}$ for $t \geq t_i$, and AGC-based reference values, $\boldsymbol{r}^{\text{AGC}}$ for $t > t_i$, where $t_0 < t_i$. Additionally, let the disturbance vector, $\boldsymbol{z}^{\text{n}}$, be composed of a pre-disturbance value, $\boldsymbol{z}^{\text{PR}}$ for $t \leq t_0$, and a post-disturbance value, $\boldsymbol{z}^{\text{PO}}$ for $t > t_0$.

## A. Economic Dispatch

In this work, the ED program leverages the IDPS dynamic model to determine the steady-state operating point for pre-disturbance conditions, ensuring that all operational and security constraints are met and that the solution remains valid for any IBR control design realization. The ED program explicitly defines the active and reactive reference signals for all IBRs, $\{\boldsymbol{p}_{\text{ref}}^{\text{ED}}, \boldsymbol{q}_{\text{ref}}^{\text{ED}}\} \in \boldsymbol{r}^{\text{ED}}$, and implicitly defines the related steady-state variables, $\boldsymbol{x}^{\text{ED}}$. Thus, let the ED program be defined as follows:

$$\min_{\{\boldsymbol{r}^{\text{ED}}, \boldsymbol{x}^{\text{ED}}\}} \Phi_{\text{ED}} \tag{23a}$$

$$\text{s.t. } \boldsymbol{f}^*(\boldsymbol{x}^{\text{ED}}, \boldsymbol{y}^{\text{ED}}, \mathcal{B}\ , \boldsymbol{z}^{\text{PR}}, \boldsymbol{r}^{\text{ED}}) = 0, \tag{23b}$$

$$\boldsymbol{g}^*(\boldsymbol{x}^{\text{ED}}, \boldsymbol{y}^{\text{ED}}, \mathcal{B}\ , \boldsymbol{z}^{\text{PR}}, \boldsymbol{r}^{\text{ED}}) = 0, \tag{23c}$$

$$\boldsymbol{h}^{\text{IBR}^*} = 0 \qquad\qquad , \boldsymbol{h}_{PQ}^{\text{IBR}} = \boldsymbol{i}_{x,dq}, \tag{23d}$$

$$\boldsymbol{v}_{dc}^{\text{IBR}} = \mathcal{V}_{dc,\text{nom}}^{\text{IBR}} \qquad , \boldsymbol{\omega}_{dq}^{\text{IBR}} = 1, \tag{23e}$$

$$\boldsymbol{v}_d^{\text{IBR}} = \mathcal{V}_{\text{nom}}^{\text{IBR}} \qquad\quad , \boldsymbol{v}_q^{\text{IBR}} = 0, \tag{23f}$$

$$\boldsymbol{p}^{\text{IBR}} = \tilde{\boldsymbol{p}}^{\text{IBR}} = \boldsymbol{p}_{\text{ref}}^{\text{ED}} \quad , \boldsymbol{q}^{\text{IBR}} = \tilde{\boldsymbol{q}}^{\text{IBR}} = \boldsymbol{q}_{\text{ref}}^{\text{ED}}, \tag{23g}$$

$$\boldsymbol{p}_{\text{ref}}^{\text{ED}\circ 2} + \boldsymbol{q}_{\text{ref}}^{\text{ED}\circ 2} \leq \mathcal{S}_{\text{nom}}^{\text{IBR}\circ 2} \quad , |\boldsymbol{i}_{x,dq}^{\text{IBR}}| \leq \mathcal{I}_{\text{nom}}^{\text{IBR}}, \tag{23h}$$

$$\mathcal{V}_{\text{min}}^{\text{N}} \leq |\boldsymbol{v}_{DQ}^{\text{N}}| \leq \mathcal{V}_{\text{max}}^{\text{N}} \quad , |\boldsymbol{i}_{DQ}^{\text{RL}}| \leq \mathcal{I}_{\text{max}}^{\text{RL}}, \tag{23i}$$

$$0 \leq \boldsymbol{\theta}_{dq}^{\text{IBR}} \leq 2\pi \qquad , v_Q^{\text{N(Slack)}} = 0, \tag{23j}$$

where in (23a), $\Phi_{\text{ED}}$ is an arbitrary objective function, typically set to minimize generation costs based on fluctuating IBR bids.

In (23b)-(23c), $\boldsymbol{f}^*$ and $\boldsymbol{g}^*$ denote the collection of differential and algebraic constraints for the IDPS physical layer variables. To ensure that the ED yields a steady-state solution for $\boldsymbol{x}^{\text{ED}}$ independent of the IBRs control layer variables, the physical state variables derivatives are set to zero in (23b).

To further ensure independence from IBRs control design, the constrains (23d)-(23g) are included. In (23d), $\boldsymbol{h}^{\text{IBR}^*}$ collects the control layer state variables, i.e., variables denoted by $h$ in Section III, except for the PQ integrator states from (18), which are gathered in $\boldsymbol{h}_{PQ}^{\text{IBR}}$. In (23e)-(23f), $\mathcal{V}_{dc,\text{nom}}^{\text{IBR}}$ and $\mathcal{V}_{\text{nom}}^{\text{IBR}}$ collect the nominal DC and AC voltages for all IBRs.

Constraints in (23h) ensure that the IBR reference signals remain within nominal operating ranges, thereby maintaining

a current headroom. Meanwhile, in (23i), nodal voltage and branch current limits are enforced to remain within their security bounds defined by $\mathcal{V}^{\mathrm{N}}_{\min}$, $\mathcal{V}^{\mathrm{N}}_{\max}$, and $\mathcal{I}^{\mathrm{RL}}_{\max}$. Finally, to avoid redundant solutions, in (23j) $\boldsymbol{\theta}_{dq}$ is bounded and the $Q$-frame voltage of an arbitrary slack bus, $v_Q^{\mathrm{N(Slack)}}$, is set to zero.

### B. Automatic Generation Control

We formulate an AGC program to mimic the AGC's typically imperfect attempt to restore nominal frequency by adjusting the generators active power reference signals, either increasing or decreasing them depending on whether the disturbance causes an Under-Frequency (UF) or Over-Frequency (OF) event, respectively. Thus, the AGC program defines the updated reference signals, $\{\boldsymbol{p}^{\mathrm{AGC}}_{\mathrm{ref}}, \boldsymbol{q}^{\mathrm{AGC}}_{\mathrm{ref}}\} \in \boldsymbol{r}^{\mathrm{AGC}}$, as follows:

$$\min_{\{\boldsymbol{r}^{\mathrm{AGC}}\}} \quad \Phi_{\mathrm{AGC}} \tag{24a}$$

$$\text{s.t.} \quad \sum \boldsymbol{p}^{\mathrm{AGC}}_{\mathrm{ref}} = \sum \boldsymbol{p}^{\mathrm{PO}}_{\mathrm{L}} \tag{24b}$$

$$\boldsymbol{p}^{\mathrm{AGC}^{\circ 2}}_{\mathrm{ref}} + \boldsymbol{q}^{\mathrm{ED}^{\circ 2}}_{\mathrm{ref}} \leq \mathcal{S}^{\mathrm{IBR}^{\circ 2}}_{\mathrm{nom}} \tag{24c}$$

$$\text{if UF event:} \quad \boldsymbol{p}^{\mathrm{AGC}}_{\mathrm{ref}} \geq \boldsymbol{p}^{\mathrm{ED}}_{\mathrm{ref}} \tag{24d}$$

$$\text{if OF event:} \quad \boldsymbol{p}^{\mathrm{AGC}}_{\mathrm{ref}} \leq \boldsymbol{p}^{\mathrm{ED}}_{\mathrm{ref}} \tag{24e}$$

$$\boldsymbol{q}^{\mathrm{AGC}}_{\mathrm{ref}} = \boldsymbol{q}^{\mathrm{ED}}_{\mathrm{ref}} \tag{24f}$$

where in (24a), $\Phi_{\mathrm{AGC}}$ is an arbitrary objective function, typically set to prioritize generators in a fluctuating merit order.

In (24b), $\sum \boldsymbol{p}^{\mathrm{PO}}_{\mathrm{L}}$ represents the post-disturbance total demand. Thus, (24b) requires the AGC to adjust active power references so that total generation matches total demand, ignoring system losses and reflecting the AGC's typically imperfect frequency regulation. Constraint (24c) ensures that the re-dispatch remains within each IBR's apparent power limits. Constraints (24d) and (24e) enforce directional adjustments of active power. Whether the event leads to an UF or OF event can be determined by including a frequency measurement tool or, simply, by comparing $\boldsymbol{z}^{\mathrm{PR}}$ with $\boldsymbol{z}^{\mathrm{PO}}$. However, this comparison depends on the nature of the disturbance and is therefore left unspecified. Finally, (24f) ensures that reactive power references are inherited from the ED solution.

### C. Dispatch Admissible Sets

The ED and AGC admissible sets are defined as:

$$\mathcal{A}^{\mathrm{ED}} = \Big\{ \{\boldsymbol{r}^{\mathrm{ED}}, \boldsymbol{x}^{\mathrm{ED}}\} \quad | \text{ (23b)-(23j) are satisfied} \Big\} \tag{25a}$$

$$\mathcal{A}^{\mathrm{AGC}} = \Big\{ \{\boldsymbol{r}^{\mathrm{AGC}}\} \quad | \text{ (24b)-(24f) are satisfied} \Big\}, \tag{25b}$$

where the objective functions as defined in (23a) and (24a) have not been incorporated.

Accordingly, within the ROCP, the admissible dispatch set is specified as:

$$\mathcal{A}^{\mathrm{r}} := \{\{\boldsymbol{r}^{\mathrm{ED}}, \boldsymbol{r}^{\mathrm{AGC}}, \boldsymbol{x}_{t_0}\} \mid \{\boldsymbol{r}^{\mathrm{ED}}, \boldsymbol{x}_{t_0}\} \in \mathcal{A}^{\mathrm{ED}} \tag{26}$$
$$\mathcal{A}^{\mathrm{ED}}, \ \boldsymbol{r}^{\mathrm{AGC}} \in \mathcal{A}^{\mathrm{AGC}}\}\}$$

## V. LARGE-SIGNAL DISTURBANCES

Large disturbances are modeled using stepwise time-varying coefficients and parameters, denoted by $\boldsymbol{z}^{\mathrm{jt}}$ and referred to as system conditions. This structure represents disturbances as discrete changes in system coefficients and parameters, allowing to model a wide range of large-signal events, such as element outages or the sudden connection or disconnection of large loads. Constraining the large-signal disturbance space is essential for producing meaningful and feasible results. Furthermore, bounding the disturbance space also enhances the computational tractability of the problem by reducing the size of the search space.

This work focuses on two classes of large-signal disturbances: the sudden connection and disconnection of large loads. In modern power systems, these disturbances are becoming increasingly relevant due to the rapid growth of large-scale facilities, most notably data centers [17], which can introduce abrupt, high-magnitude changes in demand. Such events represent critical scenarios where control design can play a pivotal role in shaping the system's dynamic response.

Thus, in this work we limit ourselves to define the admissible large-signal disturbance space for sudden load changes. Accordingly, within the ROCP, the admissible disturbance set, $\mathcal{A}^{\mathrm{z}}$, is specified as:

$$\mathcal{A}^{\mathrm{z}} = \Big\{ \{\boldsymbol{z}^{\mathrm{PR}}, \boldsymbol{z}^{\mathrm{PO}}\} \mid \boldsymbol{z}_{\mathrm{L}} \in \{0,1\}^{N_{\mathrm{L}}}, \ \sum \boldsymbol{z}_{\mathrm{L}} = 1 \ldots \tag{27a}$$
$$\ldots \mathcal{P}^{\mathrm{L}}_{\min} \leq \boldsymbol{p}^{\mathrm{PR}}_{\mathrm{L}} \leq \mathcal{P}^{\mathrm{L}}_{\max} \qquad , \ \mathcal{P}^{\mathrm{L}}_{\min} \leq \boldsymbol{p}^{\mathrm{PO}}_{\mathrm{L}} \leq \mathcal{P}^{\mathrm{L}}_{\max},$$
$$\mathcal{Q}^{\mathrm{L}}_{\min} \leq \boldsymbol{q}^{\mathrm{PR}}_{\mathrm{L}} \leq \mathcal{Q}^{\mathrm{L}}_{\max} \qquad , \ \mathcal{Q}^{\mathrm{L}}_{\min} \leq \boldsymbol{q}^{\mathrm{PO}}_{\mathrm{L}} \leq \mathcal{Q}^{\mathrm{L}}_{\max},$$
$$|\boldsymbol{p}^{\mathrm{PO}}_{\mathrm{L}} - \boldsymbol{p}^{\mathrm{PR}}_{\mathrm{L}}| \leq \boldsymbol{z}_{\mathrm{L}}^T \mathcal{P}^{\mathrm{LC}}_{\max} \quad , \ |\boldsymbol{q}^{\mathrm{PO}}_{\mathrm{L}} - \boldsymbol{q}^{\mathrm{PR}}_{\mathrm{L}}| \leq \boldsymbol{z}_{\mathrm{L}}^T \mathcal{Q}^{\mathrm{LC}}_{\max},$$
$$(\boldsymbol{p}^{\mathrm{PO}}_{\mathrm{L}} - \boldsymbol{p}^{\mathrm{PR}}_{\mathrm{L}})^T (\boldsymbol{q}^{\mathrm{PO}}_{\mathrm{L}} - \boldsymbol{q}^{\mathrm{PR}}_{\mathrm{L}}) \geq \boldsymbol{0}, \qquad \Big\}$$

where $\{\boldsymbol{p}^{\mathrm{PR}}_{\mathrm{L}}, \ \boldsymbol{q}^{\mathrm{PR}}_{\mathrm{L}}\} \in \boldsymbol{z}^{\mathrm{PR}}$ and $\{\boldsymbol{p}^{\mathrm{PO}}_{\mathrm{L}}, \ \boldsymbol{q}^{\mathrm{PO}}_{\mathrm{L}}\} \in \boldsymbol{z}^{\mathrm{PO}}$ denote the pre- and post-disturbance active and reactive power load vectors for the $N_{\mathrm{L}}$ loads in the IDPS. Furthermore, the bounds $\mathcal{P}^{\mathrm{L}}_{\min}$, $\mathcal{P}^{\mathrm{L}}_{\max}$, $\mathcal{Q}^{\mathrm{L}}_{\min}$, and $\mathcal{Q}^{\mathrm{L}}_{\max}$ define load permissible ranges, while $\mathcal{P}^{\mathrm{LC}}_{\max}$ and $\mathcal{Q}^{\mathrm{LC}}_{\max}$ set the maximum step-change value. The auxiliary binary decision variable $\boldsymbol{z}_{\mathrm{L}}$ of size $N_{\mathrm{L}}$ selects which load is allowed to change. It is further enforced that only one load is disturbed at a time.

## VI. DYNAMIC MODEL

Consider a power system with $N_{\mathrm{N}}$ nodes ($N_{\mathrm{Sh}}$ with shunt capacitors and $N_{\mathrm{NSh}}$ without shunt capacitors), $N_{\mathrm{IBR}}$ inverter-based resources, $N_{\mathrm{L}}$ loads, and $N_{\mathrm{RL}}$ lines and transformers. Define the incidence matrices:

- $\mathcal{B}_{\mathrm{Sh}}$: Indicates nodes with shunt capacitors. Matrix size $(N_{\mathrm{N}} \times N_{\mathrm{Sh}})$ with elements $b^{\mathrm{Sh}}_{k,j} \in \{0,1\}$ indicating if the $j$-th shunt capacitor is connected to the $k$-th node.

- $\mathcal{B}_{\mathrm{NSh}}$: Indicates nodes without shunt capacitors. Matrix size $(N_{\mathrm{N}} \times N_{\mathrm{NSh}})$ with elements $b^{\mathrm{NSh}}_{k,j} \in \{0,1\}$ satisfying:

$$\boldsymbol{v}^{\mathrm{N}}_D = \mathcal{B}_{\mathrm{Sh}} \boldsymbol{v}^{\mathrm{Sh}}_D + \mathcal{B}_{\mathrm{NSh}} \boldsymbol{v}^{\mathrm{NSh}}_D, \tag{28a}$$

$$\boldsymbol{v}^{\mathrm{N}}_Q = \mathcal{B}_{\mathrm{Sh}} \boldsymbol{v}^{\mathrm{Sh}}_Q + \mathcal{B}_{\mathrm{NSh}} \boldsymbol{v}^{\mathrm{NSh}}_Q, \tag{28b}$$

where $(\boldsymbol{v}^{\mathrm{N}}_D, \boldsymbol{v}^{\mathrm{N}}_Q)$, $(\boldsymbol{v}^{\mathrm{Sh}}_D, \boldsymbol{v}^{\mathrm{Sh}}_Q)$, and $(\boldsymbol{v}^{\mathrm{NSh}}_D, \boldsymbol{v}^{\mathrm{NSh}}_Q)$ are the $D$- and $Q$-frame vectors of node voltages for all nodes (size $N_{\mathrm{N}}$),

nodes with shunt capacitors (size $N_\text{Sh}$), and nodes without shunt capacitors (size $N_\text{NSh} = N_\text{N} - N_\text{Sh}$), respectively. Note that nodes containing one or more IBRs are classified as nodes without shunt capacitors, since the IBR models already include a shunt capacitor filter. If a shunt capacitor is also physically installed at an IBR-connected node, the equivalent capacitance must be computed and assigned to the IBR's filter capacitance.

- $\mathcal{B}_\text{IBR}$: Indicates nodes with IBRs. Matrix size $(N_\text{N} \times N_\text{IBR})$ with elements $b_{k,j}^\text{IBR} \in \{0, 1\}$ indicating if the $j$-th IBR is connected to the $k$-th node. IBRs are included as:

$$\boldsymbol{v}_D^\text{IBR} = \mathcal{B}_\text{IBR}^T \boldsymbol{v}_D^\text{N}, \qquad \boldsymbol{v}_Q^\text{IBR} = \mathcal{B}_\text{IBR}^T \boldsymbol{v}_Q^\text{N}, \qquad (29)$$

where $(\boldsymbol{v}_D^\text{IBR}, \boldsymbol{v}_Q^\text{IBR})$ are the $D$ and $Q$-frame vectors of IBRs node voltages (size $N_\text{IBR}$).

- $\mathcal{B}_\text{L}$: Indicates nodes with loads. Matrix size $(N_\text{N} \times N_\text{L})$ with elements $b_{k,j}^\text{L} \in \{0, 1\}$ indicating if the $j$-th load is connected to the $k$-th node.

- $\mathcal{B}_\text{RL}$: Indicates connections between nodes with either a line, a transformer, or both. Matrix size $(N_\text{N} \times N_\text{RL})$ with elements $b_{k,j}^\text{RL} \in \{-1, 0, 1\}$ indicating if the $j$-th line is connected to the $k$-th node. Positive and negative $b_{k,j}^\text{RL}$ signs define the line's current flow from node to node (positive current flows from nodes with positive sign to nodes with negative sign).

### A. Loads

Loads are included as voltage dependent current sources based on a ZIP model [2] defined as:

$$\boldsymbol{v}_D^\text{L} = \mathcal{B}_\text{L}^T \boldsymbol{v}_D^\text{N}, \qquad \boldsymbol{v}_Q^\text{L} = \mathcal{B}_\text{L}^T \boldsymbol{v}_Q^\text{N}, \tag{30a}$$

$$\boldsymbol{p}^\text{L} = \mathcal{P}_\text{L} \odot \left( \mathcal{Z}_P^a \odot |\boldsymbol{v}_{DQ}^\text{L}|^{\circ 2} + \mathcal{Z}_P^b \odot |\boldsymbol{v}_{DQ}^\text{L}| + \mathcal{Z}_P^c \right), \tag{30b}$$

$$\boldsymbol{q}^\text{L} = \mathcal{Q}_\text{L} \odot \left( \mathcal{Z}_Q^a \odot |\boldsymbol{v}_{DQ}^\text{L}|^{\circ 2} + \mathcal{Z}_Q^b \odot |\boldsymbol{v}_{DQ}^\text{L}| + \mathcal{Z}_Q^c \right), \tag{30c}$$

$$\boldsymbol{i}_D^\text{L} = \left( \boldsymbol{p}^\text{L} \odot \boldsymbol{v}_D^\text{L} + \boldsymbol{q}^\text{L} \odot \boldsymbol{v}_Q^\text{L} \right) \oslash |\boldsymbol{v}_{DQ}^\text{L}|^{\circ 2}, \tag{30d}$$

$$\boldsymbol{i}_Q^\text{L} = \left( \boldsymbol{p}^\text{L} \odot \boldsymbol{v}_Q^\text{L} - \boldsymbol{q}^\text{L} \odot \boldsymbol{v}_D^\text{L} \right) \oslash |\boldsymbol{v}_{DQ}^\text{L}|^{\circ 2}, \tag{30e}$$

where $\mathcal{Z}_P^a, \mathcal{Z}_P^b, \mathcal{Z}_P^c, \mathcal{Z}_Q^a, \mathcal{Z}_Q^b$, and $\mathcal{Z}_Q^c$ are vectors of ZIP co-efficients for the $N_\text{L}$ loads. For each load, the ZIP coefficients must satisfy $Z_P^a + Z_P^b + Z_P^c = 1$ and $Z_Q^a + Z_Q^b + Z_Q^c = 1$. The vectors $\boldsymbol{v}_D^\text{L}$ and $\boldsymbol{v}_Q^\text{L}$ represent the $D$- and $Q$-frame voltages of load buses (size $N_\text{L}$). The corresponding $D$- and $Q$-frame load currents and instantaneous active and reactive powers are collected in the vectors $\boldsymbol{i}_D^\text{L}, \boldsymbol{i}_Q^\text{L}, \boldsymbol{p}^\text{L}$, and $\boldsymbol{q}^\text{L}$, respectively. Finally, $\mathcal{P}_\text{L}$ and $\mathcal{Q}_\text{L}$ are vectors of size $N_\text{L}$ defining the active and reactive power consumption at each load.

### B. Lines and Transformers

Lines and transformers are modeled employing branch RL dynamics as:

$$\frac{1}{\omega_b} \frac{d}{dt} \boldsymbol{i}_D^\text{RL} = \mathcal{L}_\text{RL}^{\circ -1} \left( \mathcal{B}_\text{RL}^T \boldsymbol{v}_D^\text{N} - \mathcal{R}_\text{RL} \boldsymbol{i}_D^\text{RL} \right) + \boldsymbol{i}_Q^\text{RL} \tag{31a}$$

$$\frac{1}{\omega_b} \frac{d}{dt} \boldsymbol{i}_Q^\text{RL} = \mathcal{L}_\text{RL}^{\circ -1} \left( \mathcal{B}_\text{RL}^T \boldsymbol{v}_Q^\text{N} - \mathcal{R}_\text{RL} \boldsymbol{i}_Q^\text{RL} \right) - \boldsymbol{i}_D^\text{RL}, \tag{31b}$$

where $\mathcal{R}_\text{RL}$ and $\mathcal{L}_\text{RL}$ are vectors of resistance and inductance values for lines and transformers, each of size $N_\text{RL}$. Similarly,

$\boldsymbol{i}_D^\text{RL}$ and $\boldsymbol{i}_Q^\text{RL}$ are the $D$- and $Q$-frame current vectors for the RL branches, also of size $N_\text{RL}$. Note that, in practice, lumped $\pi$-section lines can be constructed by appropriately combining branch RL elements with shunt capacitors.

### C. Shunt Capacitors

The dynamics of shunt capacitors in the power system are modelled as:

$$\frac{1}{\omega_b} \frac{d}{dt} \boldsymbol{v}_D^\text{Sh} = \mathcal{C}_\text{Sh}^{\circ -1} \left[ \mathcal{B}_\text{Sh}^T \left( \mathcal{B}_\text{IBR} \boldsymbol{i}_D^\text{IBR} - \mathcal{B}_\text{RL} \boldsymbol{i}_D^\text{RL} - \mathcal{B}_\text{L} \boldsymbol{i}_D^\text{L} \right) \right] + \boldsymbol{v}_Q^\text{Sh}, \tag{32a}$$

$$\frac{1}{\omega_b} \frac{d}{dt} \boldsymbol{v}_Q^\text{Sh} = \mathcal{C}_\text{Sh}^{\circ -1} \left[ \mathcal{B}_\text{Sh}^T \left( \mathcal{B}_\text{IBR} \boldsymbol{i}_Q^\text{IBR} - \mathcal{B}_\text{RL} \boldsymbol{i}_Q^\text{RL} - \mathcal{B}_\text{L} \boldsymbol{i}_Q^\text{L} \right) \right] - \boldsymbol{v}_D^\text{Sh}, \tag{32b}$$

where $\mathcal{C}_\text{Sh}$ is a vector of shunt capacitance values, with size $N_\text{Sh}$. Note that if multiple capacitors are connected to a single node, they should be represented by a single equivalent capacitor with the corresponding parallel capacitance.

For nodes without shunt capacitors, the sum of currents must be zero. Thus:

$$0 = \mathcal{B}_\text{Nsh}^T \left( \mathcal{B}_\text{IBR} \boldsymbol{i}_D^\text{IBR} - \mathcal{B}_\text{RL} \boldsymbol{i}_D^\text{RL} - \mathcal{B}_\text{L} \boldsymbol{i}_D^\text{L} \right), \tag{33a}$$

$$0 = \mathcal{B}_\text{Nsh}^T \left( \mathcal{B}_\text{IBR} \boldsymbol{i}_Q^\text{IBR} - \mathcal{B}_\text{RL} \boldsymbol{i}_Q^\text{RL} - \mathcal{B}_\text{L} \boldsymbol{i}_Q^\text{L} \right). \tag{33b}$$

### D. Overview

The introduced IDPS dynamic model describes the time evolution of system variables. State variables are henceforth collected in the vector $\boldsymbol{x}_t$, and their governing differential equations are represented by the function $\boldsymbol{f}^\text{x}(\cdot)$. Algebraic states are collected in the vector $\boldsymbol{y}_t$ and algebraic constraint equations are represented by the function $\boldsymbol{f}^\text{y}(\cdot)$.

To simulate the IDPS, the following components are required:

1) **Initial state values:** Initial values of the state variables are collected in the vector $\mathcal{X}_0$.
2) **System parameters:** Fixed coefficients and parameters of power system elements are collected in the set $M^\text{PS}$.
3) **Disturbance inputs:** Stepwise time-varying coefficients and parameters used to model disturbances are collected in the vector $\boldsymbol{z}^\text{Ɫ}$.
4) **Reference signals:** Stepwise time-varying active and reactive power reference signals for each IBR, denoted by $\boldsymbol{p}_\text{ref}$ and $\boldsymbol{q}_\text{ref}$, are collected in the vector $\boldsymbol{r}^\text{Ɫ}$.
5) **Control structure configuration:** Integer indicators specifying the selected control structure for each IBR, as introduced in Section III-B2, are collected in $\boldsymbol{u}$.
6) **Tunable control parameters:** Parameters associated with the selected control structure of each IBR, as introduced in Section III-B2, are stored in $\boldsymbol{K}$.

With these components, the IDPS model can be expressed as:

$$\frac{d}{dt} \boldsymbol{x}_t = \boldsymbol{f}^\text{x}(\boldsymbol{x}_t, \boldsymbol{y}_t; \boldsymbol{u}, \boldsymbol{K}, \boldsymbol{z}_t^\text{Ɫ}, \boldsymbol{r}_t^\text{Ɫ}, M^\text{PS}), \tag{34a}$$

$$0 = \boldsymbol{f}^\text{y}(\boldsymbol{x}_t, \boldsymbol{y}_t; \boldsymbol{u}, \boldsymbol{K}, \boldsymbol{z}_t^\text{Ɫ}, \boldsymbol{r}_t^\text{Ɫ}, M^\text{PS}), \tag{34b}$$

$$\boldsymbol{x}_{t_0} = \mathcal{X}_0, \tag{34c}$$

where (34a) represents the set of Ordinary-Differential-Equations (ODEs) that govern the system's evolution, (34b) represents the set of algebraic constraints, and (34c) specifies the initial state values.

Traditionally, power system dynamics are modeled as DAE systems by including algebraic constraints $\boldsymbol{f}^{\text{y}}(\cdot)$ to satisfy Kirchhoff's laws and maintain power flow balance. However, it is often straightforward, and advantageous for ease of simulation, to reformulate the DAE system as an equivalent ODE system [18]. The complexity of this transformation depends on the characteristics of the IDPS. For further details, we refer the reader to [18], [19].

The introduced IDPS model accurately captures the transient behavior of multi-IBR power systems. Simulations based on this formulation yield results consistent with detailed three-phase $abc$ electromagnetic transient (EMT) models [7], under the assumptions defined in Section II-B. The IDPS model has been implemented in MATLAB SIMULINK and is available at: **https://github.com/Aerlio/ROC-of-IDPS**.

## VII. OBJECTIVE FUNCTION

The objective function of the ROCP plays a foundational role in the optimization framework, as it fundamentally dictates the behavior of the resulting control design. Defining an objective function that characterizes the desired behavior of an IDPS is inherently non-trivial and involves a degree of subjectivity. Its structure determines what system responses are prioritized, whether, frequency recovery, voltage regulation, damping, or control effort, and thus directly influences which control design and worst-case scenario emerge as a solution. Beyond capturing key performance objectives such as stability, resilience, controllability, or disturbance rejection, the formulation must balance computational tractability with modeling completeness.

In this work, the objective function is intentionally kept simple to enable a focused evaluation of dynamic control performance while avoiding unnecessary numerical complexity. Thus, we adopt a objective function defined as the time integral of the continuous-time expression:

$$\psi = \frac{1}{t_f - t_0} \sum_{g=1}^{N_{\text{IBR}}} \left[ (p_{t,g}^{\text{ref}} - p_{t,g})^2 + (q_{t,g}^{\text{ref}} - q_{t,g})^2 \right], \quad (35)$$

where $t_0$ and $t_f$ are the initial and final times of study, respectively. Moreover, $p_{t,g}$ and $q_{t,g}$ represent the active and reactive power injections of the $g$-th IBR at time $t$, respectively. The signals $p_{t,g}^{\text{ref}}$ and $q_{t,g}^{\text{ref}}$ are the corresponding reference trajectories.

Thus, the defined objective function measures the aggregated IBRs deviation from the active and reactive power reference signals over time, thereby promoting accurate tracking under worst-case operating conditions. Accordingly, within the ROCP, the dynamic error is quantified through a time-integrated metric of the form:

$$\Psi = \int_{t_0}^{t_f} \psi(\boldsymbol{x}_t, \boldsymbol{y}_t, \dots) \, dt, \quad (36)$$

where $t_0$ and $t_f$ are the initial a final times of analysis.

## VIII. THE ROBUST OPTIMAL CONTROL PROBLEM

All components required to construct the robust optimal control problem (ROCP) of the associated manuscript [1] have now been defined. For completeness and clarity, the ROCP is restated below in its general form, consolidating the modeling elements presented herein into a unified optimization framework. The resulting formulation constitutes the complete ROCP underlying the main manuscript [1].

The ROCP is formulated in general form as:

$$\min_{\{\boldsymbol{u}, \boldsymbol{K}\}} \max_{\{\boldsymbol{z}^{\text{PR}}, \boldsymbol{z}^{\text{PO}}, \boldsymbol{r}^{\text{ED}}, \boldsymbol{r}^{\text{AGC}}, \boldsymbol{x}_{t_0}\}} \Psi \quad (37a)$$

subject to

$$\forall t \in [t_0, t_f] : \frac{d}{dt} \boldsymbol{x}_t = \boldsymbol{f}^{\text{x}}(\boldsymbol{x}_t, \boldsymbol{y}_t; \boldsymbol{u}, \boldsymbol{K}, \boldsymbol{z}_t^{\text{r}}, \boldsymbol{r}_t^{\text{r}}, M^{\text{PS}}), \quad (37b)$$

$$\forall t \in [t_0, t_f] : \quad 0 = \boldsymbol{f}^{\text{y}}(\boldsymbol{x}_t, \boldsymbol{y}_t; \boldsymbol{u}, \boldsymbol{K}, \boldsymbol{z}_t^{\text{r}}, \boldsymbol{r}_t^{\text{r}}, M^{\text{PS}}), \quad (37c)$$

$$\forall t \in [t_0, t_f] : \quad \boldsymbol{z}_t^{\text{r}} = \boldsymbol{z}^{\text{PR}} + f_t^{\mu}(t_0)(\boldsymbol{z}^{\text{PO}} - \boldsymbol{z}^{\text{PR}}), \quad (37d)$$

$$\forall t \in [t_0, t_f] : \quad \boldsymbol{r}_t^{\text{r}} = \boldsymbol{r}^{\text{ED}} + f_t^{\mu}(t_i)(\boldsymbol{r}^{\text{AGC}} - \boldsymbol{r}^{\text{ED}}), \quad (37e)$$

$$\boldsymbol{u} \in \mathcal{A}^{\text{u}}, \qquad \boldsymbol{K} \in \mathcal{A}^{\text{K}}, \quad (37f)$$

$$\{\boldsymbol{z}^{\text{PR}}, \boldsymbol{z}^{\text{PO}}\} \in \mathcal{A}^{\text{z}}, \quad \{\boldsymbol{r}^{\text{ED}}, \boldsymbol{r}^{\text{AGC}}, \boldsymbol{x}_{t_0}\} \in \mathcal{A}^{\text{r}}. \quad (37g)$$

The objective function is defined in Section VII, and the DAE-based dynamic model of the IDPS is introduced in Section VI. The admissible sets $\mathcal{A}^{\text{u}}$, $\mathcal{A}^{\text{K}}$, $\mathcal{A}^{\text{z}}$, and $\mathcal{A}^{\text{r}}$ are specified in (20), (22), (26), and (27a), respectively.

This document provides a detailed and self-contained mathematical specification of the modeling assumptions, admissible sets, and performance criteria that define the ROCP. The above formulation therefore serves as the foundational reference for the robust control design framework developed in the main work [1].

## REFERENCES

[1] T. Ochoa, B. Chaudhuri, and M. O'Malley, "Optimal control for robust dynamic performance in inverter-dominated power systems." *Authorea Preprints*, 2026.

[2] A. Arif, Z. Wang, J. Wang, B. Mather, H. Bashualdo, and D. Zhao, "Load modeling—a review," *IEEE Transactions on Smart Grid*, vol. 9, no. 6, pp. 5986–5999, 2017.

[3] A. Yazdani and R. Iravani, *Voltage-sourced converters in power systems: modeling, control, and applications*. John Wiley & Sons, 2010.

[4] F. Dörfler and D. Groß, "Control of low-inertia power systems," *Annual Review of Control, Robotics, and Autonomous Systems*, vol. 6, pp. 415–445, 2023.

[5] A. Tayyebi, D. Groß, A. Anta, F. Kupzog, and F. Dörfler, "Frequency stability of synchronous machines and grid-forming power converters," *IEEE Journal of Emerging and Selected Topics in Power Electronics*, vol. 8, no. 2, pp. 1004–1018, 2020.

[6] P. Kundur, "Power system stability," *Power system stability and control*, vol. 10, pp. 7–1, 2007.

[7] D. Venkatramanan, M. K. Singh, O. Ajala, A. Dominguez-Garcia, and S. Dhople, "Integrated system models for networks with generators & inverters," *arXiv preprint arXiv:2203.08253*, 2022.

[8] C. J. O'Rourke, M. M. Qasim, M. R. Overlin, and J. L. Kirtley, "A geometric interpretation of reference frames and transformations: dq0, clarke, and park," *IEEE Transactions on Energy Conversion*, vol. 34, no. 4, pp. 2070–2083, 2019.

[9] S. Geng and I. A. Hiskens, "Unified grid-forming/following inverter control," *IEEE Open Access Journal of Power and Energy*, vol. 9, pp. 489–500, 2022.

[10] H. Zhang, W. Xiang, W. Lin, and J. Wen, "Grid forming converters in renewable energy sources dominated power grid: Control strategy, stability, application, and challenges," *Journal of modern power systems and clean energy*, vol. 9, no. 6, pp. 1239–1256, 2021.

[11] B. B. Johnson, T. Roberts, O. Ajala, A. D. Domínguez-García, S. V. Dhople, D. Ramasubramanian, A. Tuohy, D. Divan, and B. Kroposki, "A generic primary-control model for grid-forming inverters: Towards interoperable operation & control." in *HICSS*, 2022, pp. 1–10.

[12] N. Baeckeland, D. Chatterjee, M. Lu, B. Johnson, and G.-S. Seo, "Overcurrent limiting in grid-forming inverters: A comprehensive review and discussion," *IEEE Transactions on Power Electronics*, 2024.

[13] S. Hänggi, J. Frey, S. Van Dooren, M. Diehl, and C. H. Onder, "A modular approach for diesel engine air path control based on nonlinear mpc," *IEEE Transactions on Control Systems Technology*, vol. 31, no. 4, pp. 1521–1536, 2022.

[14] W. W. Baker, "Control, modeling, and analysis of inverter-based resources," Ph.D. dissertation, Auburn University, 2021.

[15] O. I. Elgerd and C. E. Fosha, "Optimum megawatt-frequency control of multiarea electric energy systems," *IEEE transactions on power apparatus and systems*, no. 4, pp. 556–563, 1970.

[16] G. Zhang, J. McCalley, and Q. Wang, "An agc dynamics-constrained economic dispatch model," *IEEE Transactions on Power Systems*, vol. 34, no. 5, pp. 3931–3940, 2019.

[17] K. M. U. Ahmed, M. H. Bollen, and M. Alvarez, "A review of data centers energy consumption and reliability modeling," *IEEE access*, vol. 9, pp. 152 536–152 563, 2021.

[18] H. T. Tran, H. T. Nguyen, L. T. Vu, and S. T. Ojetola, "Solving differential-algebraic equations in power system dynamic analysis with quantum computing," *Energy Conversion and Economics*, vol. 5, no. 1, pp. 40–53, 2024.

[19] U. M. Ascher and L. R. Petzold, *Computer methods for ordinary differential equations and differential-algebraic equations*. SIAM, 1998.